photonics

MDPI

Communication

Improving Low-Dispersion Bandwidth of the Silicon Photonic Crystal Waveguides for Ultrafast Integrated Photonics

Jinghan Pan [1,†], Meicheng Fu [1,†], Wenjun Yi [1], Xiaochun Wang [1], Ju Liu [1,2], Mengjun Zhu [1], Junli Qi [1], Shaojie Yin [3], Guocheng Huang [1], Shuyue Zhu [1], Xin Chen [1], Wusheng Tang [4], Jiali Liao [5], Heng Yang [6] and Xiujian Li [1,*]

[1] College of Liberal Arts and Sciences, National University of Defense Technology, Changsha 410073, China; panjinghan18@nudt.edu.cn (J.P.); fumeicheng10@nudt.edu.cn (M.F.); yiwenjun@nudt.edu.cn (W.Y.); xiaochunwang01@163.com (X.W.); liujjj801@163.com (J.L.); zhumengjun18@nudt.edu.cn (M.Z.); qijunli_r@nudt.edu.cn (J.Q.); hgc@nudt.edu.cn (G.H.); zhushuyue20@nudt.edu.cn (S.Z.); zndxcx1996@163.com (X.C.)
[2] Hunan Institute of Traffic Engineering, Hengyang 421099, China
[3] School of Electrical Engineering, Yanshan University, Qinhuangdao 066004, China; yinshaojie@stumail.ysu.edu.cn
[4] College of Meteorology and Oceanology, National University of Defense Technology, Changsha 410073, China; tangwusheng@nudt.edu.cn
[5] School of Physics and Optoelectronic Engineering, Xidian University, Xi'an 710071, China; liaojiali@xidian.edu.cn
[6] College of Information and Communication, National University of Defense Technology, Changsha 410073, China; hengy@yeah.net
* Correspondence: xjli@nudt.edu.cn
† These authors contributed equally to this work.

Citation: Pan, J.; Fu, M.; Yi, W.; Wang, X.; Liu, J.; Zhu, M.; Qi, J.; Yin, S.; Huang, G.; Zhu, S.; et al. Improving Low-Dispersion Bandwidth of the Silicon Photonic Crystal Waveguides for Ultrafast Integrated Photonics. *Photonics* **2021**, *8*, 105. https://doi.org/10.3390/photonics8040105

Received: 9 March 2021
Accepted: 31 March 2021
Published: 6 April 2021

Abstract: We design a novel slow-light silicon photonic crystal waveguide which can operate over an extremely wide flat band for ultrafast integrated nonlinear photonics. By conveniently adjusting the radii and positions of the second air-holes rows, a flat slow-light low-dispersion band of 50 nm is achieved numerically. Such a slow-light photonic crystal waveguide with large flat low-dispersion wideband will pave the way for governing the femtosecond pulses in integrated nonlinear photonic platforms based on CMOS technology.

Keywords: silicon photonics; photonic crystal waveguides; slow light

1. Introduction

With the capabilities in flexible designability, high integration and mature mass-production, the slow-light photonic crystal waveguide (PhCW) [1] has become a versatile element for many applications including integrated lasers [2], microwave photonics [3], optical communications and optical computing [4]. Especially, due to its remarkable slow-light enhanced effects and flexible dispersion engineering properties under the room-temperature condition, ultrafast nonlinear photonics within the slow-light region of PhCW has emerged as a hot topic recently, with many impressive works including front-induced transitions [5], pulse acceleration [6], pure-quartic solitons [7], pulse compression [8], ultrafast time delay tuning [9], slow-light-induced Doppler shift [10], optical auto-correlator [11] and dynamic control [12] having been demonstrated in PhCW. However, the inherent original small bandwidth, extremely large group velocity dispersion (GVD) and sophisticated linear and nonlinear loss properties distort the ultrashort pulse seriously, which limit the practical ultrafast utilization of slow-light PhCW.

Several attempts had been made to design a suitable PhCW for various broadband applications, and the performance is usually evaluated by the normalized delay-bandwidth product (NDBP), which is defined as the product of group index (N_g) and normalized bandwidth. We can obtain large NDBP by using dispersion engineering methods such as adjust-

ing structure parameters of the PhCW in symmetric or asymmetric ways [13], changing the waveguides width [14], modifying the air-hole radius [15], shifting the air-holes lattices [16], chirping the waveguides structure [17], changing the shape of holes [18], algorithmic-based inverse design approach [19] and so on. Recently, an optimized coupled-cavity PhCW with tunable capabilities and NDBP above 0.8 even had been demonstrated [20]. However, besides these theoretically achievements, from Table 1, which is a brief summary of some typical dispersion engineering PhCW that had been exploited in ultrafast photonic applications, we can find out that moderate group indexes and bandwidths are usually focused on. There are three major factors limiting the usage of higher group index in practice. The first factor is the loss scaling law, i.e., the N_g^2-dependent linear loss, though there are some preliminary methods to address this problem, such as the Bloch mode engineering [21], where the key point is to drive the electric field away from the air-holes. The second factor is the disordered transmission spectrum in the large group index region resulting from the wavelength-dependent insertion loss. Furthermore, the third factor is the high nonlinear absorption resulting from the slow-light enhanced two-photon absorption (TPA) and free-carriers absorption (FCA) [22]. What is more, combining with the high group index, large low-dispersion bandwidth is also vital for the ultrafast nonlinear photonics, as an ideal transform-limited Gaussian pulse with center wavelength of 1550 nm and 100 fs pulse-duration is corresponding to 35 nm spectral-width [23].

In practice, it is highly desirable to design a dispersion engineering slow-light silicon PhCW (Si-PhCW) with low-dispersion and wide bandwidth for ultrafast integrated nonlinear photonic applications over a wide flat band (larger than 35 nm). Usually, PhCW with group index around 10 is suitable [8,22], which can show various temporal and spectral domain phenomenon. Herein, the simulation results show that, by adjusting the radius and the lattice positions of the second air-holes rows of the standard W1 Si-PhCW, low-dispersion operating bandwidth up to 50 nm can be achieved; such a broadband Si-PhCW can be effectively applied for pulse compression [8], true time-delay [9], highly efficient field-matter interaction [24] and many other applications.

Table 1. Typical Dispersion Engineering PhCW Used in the Ultrafast Integrated Photonics.

References	N_g	Bandwidth (nm)
Front-induced transitions [5]	30	12
Optical pulse compression [8]	9	15
Ultrafast time delay tuning [9]	35	6
Optical auto-correlator [11]	30	15

2. Improving the Low-Dispersion Bandwidth by Adjusting the Lattice Positions and Radii

The novel structure is achieved by starting from a standard triangular W1 Si-PhCW, as shown in Figure 1. We use the plane wave expansion method (PWE) implemented in the MPB code [25,26] to find out the optimum design parameters, and the dispersion relationships of the transverse electric (TE) polarized mode in various engineered waveguides are calculated by using two-dimensional simulations with effective index of 2.9 [27]. In the novel structure, the lattice constant is a, the air-holes' radius (R) is $0.26a$ and the radius of the second air-holes rows (R2) is decreased and the corresponding positions are also shifted along the line defect direction by Δx.

It is helpful to get some hints from the dispersion profiles and the field distribution pattern of the unperturbed structure [15,28] for further structure engineering. We use a two-step strategy to achieve the design parameters for wide flat band, i.e., expanding the frequency range and then tailoring the dispersion profile to straight line. To expand the frequency range, one would expect to move down the dispersion profile corresponding to the K = 0.5 (gap-guided mode) as shown in Figure 2a, while making the counterpart of K = 0.35 (index-guided mode) remain unchanged. Actually, based on the variational principle [28], typically, we can achieve a smaller eigenfrequency if the field confinement in

the air-holes is smaller, and we can reduce the air-holes radius of the first rows to increase the effective index and decrease the eigenfrequency of the eigenmode [29]. However, according to the field distribution as shown in Figure 2b, the first rows of air-holes adjacent to the line defect have strong impact on both the gap-guided and the index-guided modes region, so if we decrease the first rows' radius, the dispersion profiles of both the gap-guided mode and index-guided mode will be moved down together. As for the third and other rows far away from the line defect, there is a relatively small field strength, which makes them also have a smaller impact on the dispersion than the second rows, and here, we focus on expanding the bandwidth effectively by adjusting structure parameters as less as possible, although the third and fourth rows can also be hired as a knob to fine tailor the dispersion as in Ref. [30], the achieved bandwidth is only around 10nm. Hence, we choose to only decrease the radius of the second air-holes rows firstly. The simulation results in Figure 3 show that the gap-guided mode lower faster than the index-guided mode as we expected. It should be particularly pointed out that this step is vital for designing an extremely wide flat band PhCW.

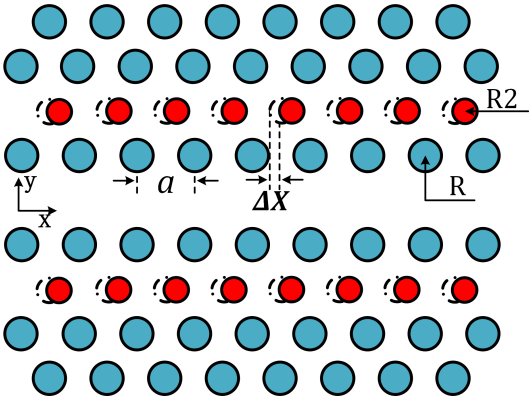

Figure 1. Schematic of the dispersion engineering slow-light Si-PhCW, the blue circles represent the air-holes in a standard W1 PhCW with a lattice constant of a, while the red circles represent the engineered air-holes, i.e., decreasing the radius from R to R2 and shifting horizontally from the dashed circles by Δx.

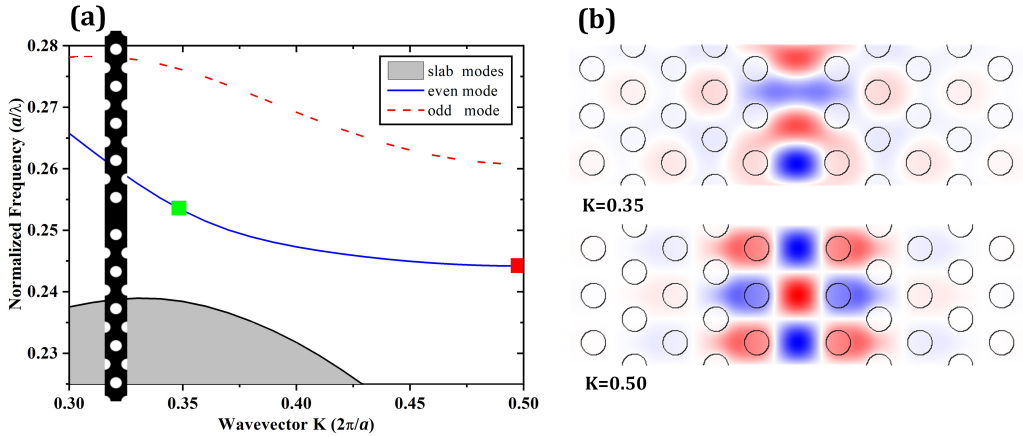

Figure 2. (**a**) Dispersion relationship of the unperturbed standard W1 Si-PhCW, the inset represents the supercell used in MPB, (**b**) Hz field distribution corresponding to TE polarization at K = 0.35 (green diamond in (**a**)) and K = 0.5 (red diamond in (**a**)), respectively.

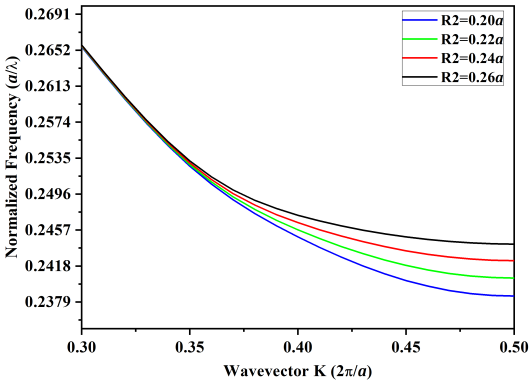

Figure 3. Dispersion profiles of the guided mode for various R2.

In order to expand the frequency bandwidth corresponding to this K range, for the first glance, one may expect to move up or down the band in K = 0.5, but it is likely to result in the multimode problem by the former routine, which is the case of Ref. [31]. Therefore, we choose to use the later routine, and as shown in Figure 3, the corresponding frequency bandwidth of the target K range can be greatly enlarged when R2 = 0.20a and 0.22a.

After the successfully expanding of the K range, the second step is to fine-tune the dispersion profile to a straight-line shape, which means the vanishment of the group dispersion. Furthermore, the appearance of the straight dispersion profiles indicates the increasing group index of the index-guided mode and the decreasing group index of the gap-guided mode, which result in a high group index band with low dispersion. Among the methods mentioned in the introduction, here we choose to shift the positions of the radius-decreased air-holes along the line defect direction. Compared with the structures proposed previously, our design only changes the parameters of the second air-holes rows, which is highly desired for the practical fabrication processes.

3. Results and Discussion

Figure 4 shows the simulation results by combining the decreased R2 = 0.20a and various lattice shifted distance of the second air-holes rows to tune the parabolic dispersion profiles in Figure 3 to an almost straight line. Figure 4 shows that the dispersion profiles will gradually move up and eventually turn to a straight profile when Δx = 0.20a. The calculated group index and GVD parameters corresponding to Figure 4 are shown in Figure 5a,b. In order to make the waveguide work around 1550 nm, we have set the lattice constant a = 380 nm here. When $\Delta x = 0.25a$, as the magenta solid line shown in Figure 5a, the group index keeps around 9 over an extremely wide band almost covering from 1520 nm to 1570 nm, i.e., bandwidth up to 50 nm, what should be pointed out is that although the group index corresponding to $\Delta x = 0.25a$ seems to be varied largely, but this is resulting from the small vertical scale range, which is only 4 over the whole wavelength range. The GVD parameters give a convincing picture to address this illusion, as shown in Figure 5b, over a wide wavelength range from 1520 nm to 1570 nm, the GVD is keep below 1000 ps^2/m, which is really a quite small value for a dispersion tailored PhCW.

For the ultrafast integrated photonics, it is important to investigate the optimized parameters range for the designed structures, here we have further simulated the results where R2 = 0.22a, and the other parameters are the same as Figure 5. The group index and GVD are shown in Figure 6a,b, respectively. Because of the larger hole radius, the group index has a higher value around 12 and a higher GVD compared with the case of R2 = 0.20a. However, the GVD is still below 2000 ps^2/m over wavelength range from 1510 nm to 1565 nm, and the main parts are below 1000 ps^2/m; what is more, the low dispersion wavelength range is basically located in the same positions for all the simulations, which is quite significant for the dispersion engineered PhCW. Combing the results in Figures 5 and 6, it is convincing to say that our design has an outstanding performance over a robust optimized parameters range. In practical use and fabrication, the most

important thing of PhCW is to keep the target working wavelength and performance stable even though taking the fabrication errors into consideration. We can see that a quite stable working wavelength around 1550 nm can always be achieved in Figures 5 and 6 when the R2 and Δx vary from 0.2a to 0.22a and 0a to 0.25a, respectively. Furthermore, the N_g also only change a little around 10 when R2 and Δx vary from 0.2a to 0.22a and 0.2a to 0.22a, respectively. In conclusion, the target working wavelength and N_g can be well maintained with fabrication errors around 10 nm, which is achievable for the nanofabrication facilities.

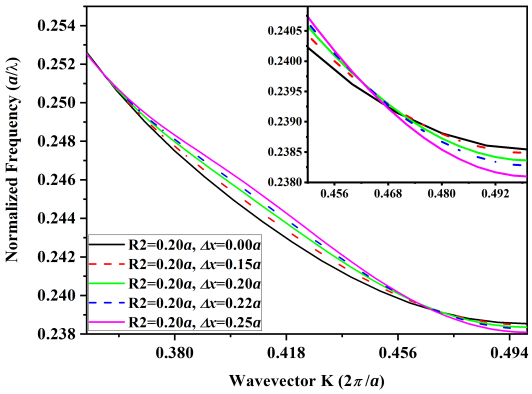

Figure 4. Dispersion profiles corresponding to R2 = 0.20a, while Δx is variable, the inset shows partially zoomed-in lines.

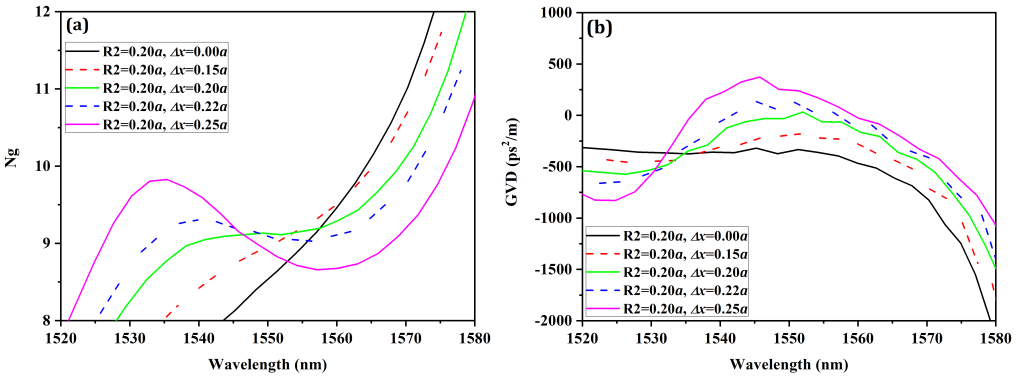

Figure 5. (**a**) The calculated group index and (**b**) Calculated GVD parameters, where R2 = 0.20a and a is equal to 380 nm.

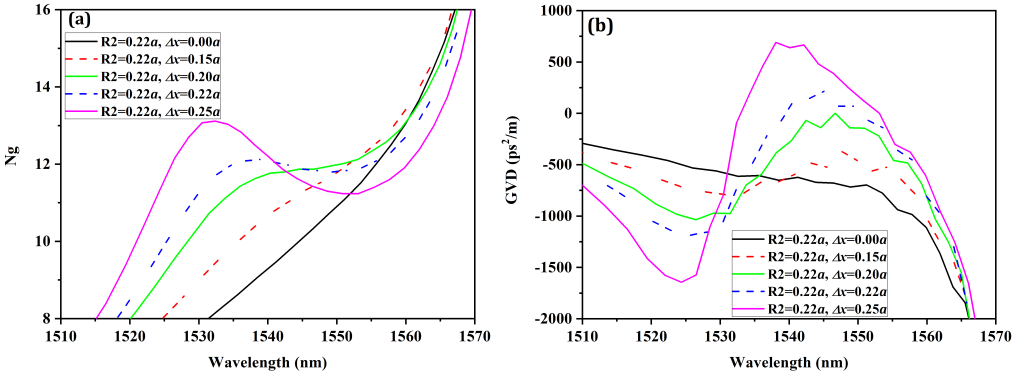

Figure 6. (**a**) The calculated group index and (**b**) Calculated GVD parameters, where R2 = 0.22a and a is equal to 380 nm.

Furthermore, we have performed the simulation by the two-dimensional finite-dimensional time-domain (FDTD) to verify the PWE results, where a transform limited Gaussian pulse with full-width half-maximum (FWHM) of 200 fs and center wavelength

of 1550 nm was used, and the input pulse spectrum is shown in Figure 7a. With two time domain monitors standing 80a (a = 380 nm) apart are used for recording the transmission signal, the simulation results are shown in Figure 7. As shown in Figure 7b, where the PhCW is a standard W1 waveguide, the simulated result shows the pulse has been broaden seriously by the dispersion. For the dispersion tailored PhCW shown in Figure 7c, where the radius of the second air-holes rows is 0.22a and the lattice-shifted distance is 80 nm, the pulse broaden phenomenon is well suppressed. The group velocity and group index can also be extracted from Figure 7c, which are 2.4×10^7 m/s and 12.5 and well agreed with the results in Figure 6a.

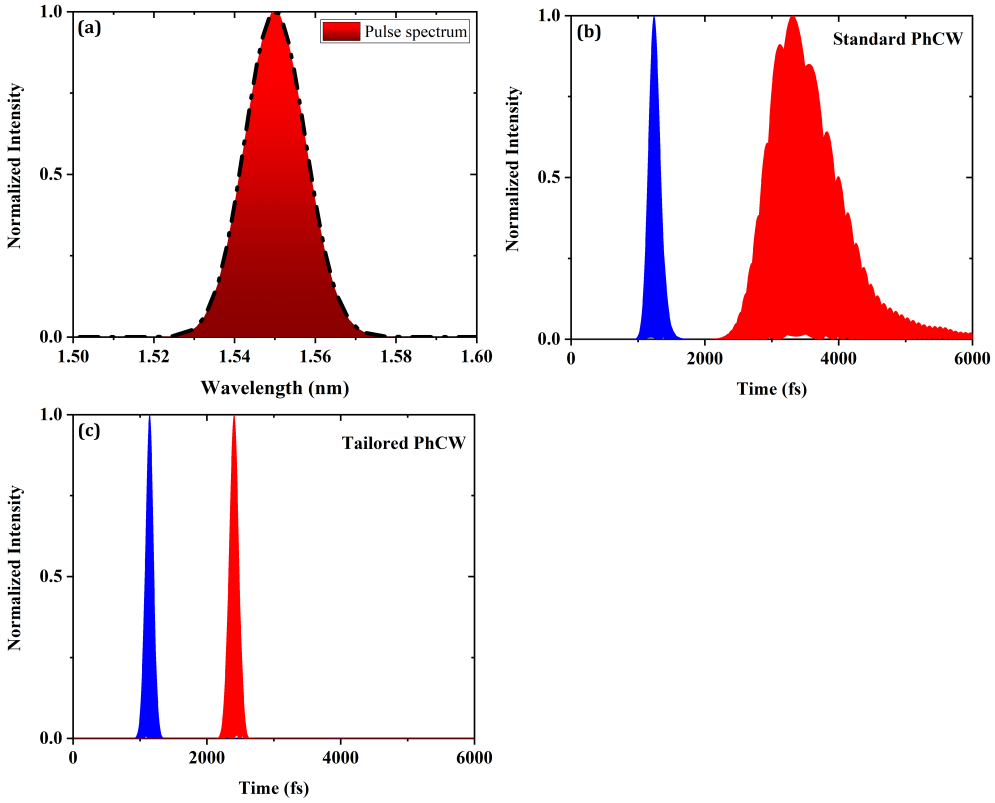

Figure 7. (**a**) Spectrum of the input pulse, and the temporal pulse profiles for (**b**) standard PhCW and (**c**) tailored PhCW at two selected detection points at 10a and 90a, when R2 = 0.22a and Δx = 80 nm.

In Figure 8, we have done a three-dimensional (3-D) FDTD simulation to further validate our 2-D results and guide the fabrication of our design. Here, a typical silicon-on-insulator (SOI) air-bridge PhCW with thickness of 220 nm has been used, and because the thickness of the SOI is fixed, the choice of other parameters have also been affected comparing with the 2-D simulation. During the simulation, a lattice period of 400 nm, radius (R) of 100 nm have been used to set the working wavelength near 1550 nm, and the corresponding R2 and Δx are a little different from the 2-D simulation. However, as shown in Figure 8a, the low dispersion bandwidth can also be effectively expanded by reducing the R2, and the values of N_g and low dispersion bandwidth are also similar with the 2-D simulations as shown in Figure 8b,c. By using the 3-D FDTD method, we have also presented the electric field profiles corresponding to the cases of $R2 = 0.16a, \Delta x = 0$ nm and $R2 = 0.16a, \Delta x = 100$ nm in Figure 8. We can find out that the field confinement in the air-holes becomes larger by comparing Figure 9a–d, which also verify our design principles presented in Section 2.

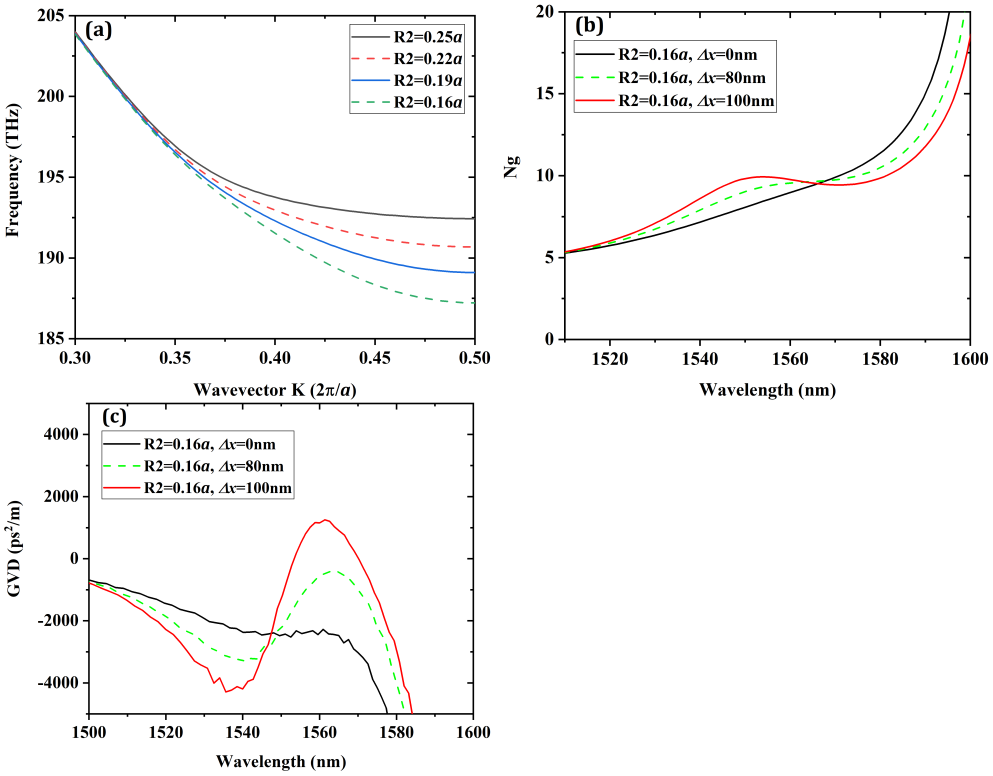

Figure 8. (**a**) Dispersion profiles of the guided mode for various R2, (**b**) the group index and (**c**) GVD parameters for various R2 and Δx. The thickness of the silicon film in this 3-D FDTD simulation is 220 nm, the lattice period a is 400 nm and the radius R is 100 nm, while the $R2$ and Δx values are shown in the legends.

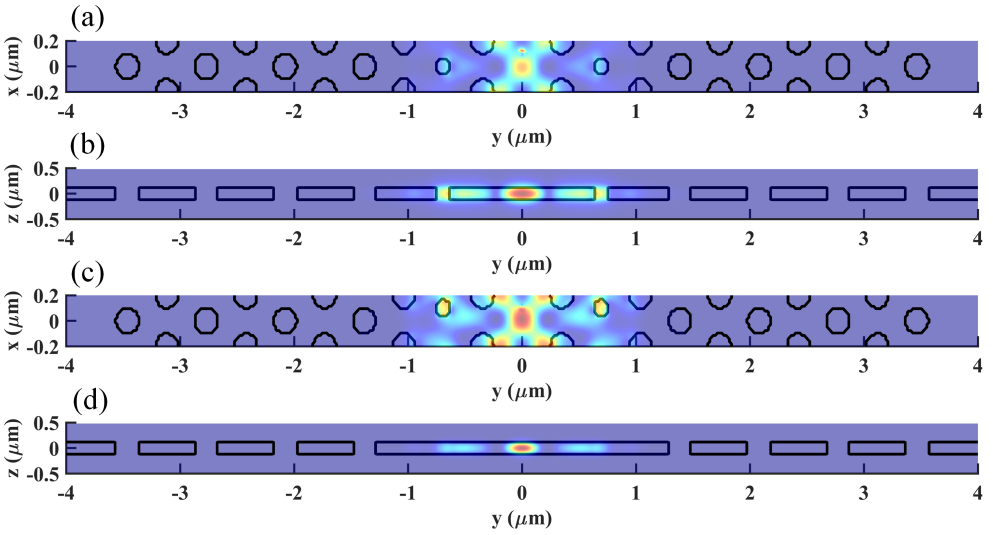

Figure 9. The electric field profiles for different structure parameters and observation planes, i.e., z = 0 plane for (**a**,**c**), x = 0 plane for (**b**,**d**). While R2 = 0.16a, Δx = 0 nm in (**a**,**b**), R2 = 0.16a, Δx = 100 nm in (**c**,**d**). The definition of the axes has been given in Figure 1.

4. Conclusions

In summary, a novel slow light Si-PhCW with extremely wide flat band and low dispersion has been designed. By conveniently adjusting the radius and lattice positions of the second air-holes rows, an extremely wide flat band up to larger than 50 nm covering almost the whole c-band is obtained. For the case of R2 = 0.20a and Δx = 0.25a, the group index is about 10, and the variable span of group index is only 3 over a bandwidth larger

than 50 nm. We highlight the method to expand the corresponding frequency band by lowering the dispersion band within the counterpart K range, and here the method has the potential to be effectively applied for other similar structures. For the femtosecond laser pulse applications in the various microstructure waveguides as photonic crystal waveguides and photonic crystal fibers, the complicated dispersion will play a crucial role. By lowering the dispersion over an extremely wide band, the ultrafast femtosecond pulses will undergo a smaller dispersion-induced pulse-width expanding, and then will experience better nonlinear slow light enhanced effects. At the same time, by combining the depressed GVD and the remarkable nonlinear matter-light interaction, the higher-order nonlinear effects and the higher-order dispersion will come to be prominent, then many further interesting phenomena will become easier to catch. Anyway, our design method has demonstrated a regular pattern to design a PhCW with an extremely wide flat band.

Author Contributions: Conceptualization, M.F. and X.L.; software, M.F. and S.Y.; investigation, J.P., and M.F.; writing, all authors; supervision, X.L. All authors have read and agreed to the published version of the manuscript.

Funding: This research was funded by the Natural Science Foundation of Hunan Province (2019JJ40341); Natural Science Foundation of China (11704411, 62005207, 62005317); Natural Science Foundation of Shaanxi Province (2019JQ-648) and No.61404160205.

Institutional Review Board Statement: Not applicable.

Informed Consent Statement: Not applicable.

Data Availability Statement: Not applicable.

Conflicts of Interest: The authors declare no conflict of interest.

References

1. Baba, T. Slow light in photonic crystals. *Nat. Photonics* **2008**, *2*, 465–473. [CrossRef]
2. Jesper, M.; Yi, Y.; Thorsten, S.R.; Elizaveta, S.; Kresten, Y. Semiconductor Fano Lasers. *IEEE J. Sel. Top. Quant.* **2019**, *25*, 1–14.
3. Sancho, J.; Bourderionnet, J.; Lloret, J.; Combrié, S.; Gasulla, I.; Xavier, S.; Sales, S.; Colman, P.; Lehoucq, G.; Dolfi, D.; et al. Integrable microwave filter based on a photonic crystal delay line. *Nat. Commun.* **2012**, *3*, 1075. [CrossRef] [PubMed]
4. Nozaki, K.; Shinya, A.; Matsuo, S.; Suzaki, Y.; Segawa, T.; Sato, T.; Kawaguchi, Y.; Takahashi, R.; Notomi, M. Ultralow-power all-optical RAM based on nanocavities. *Nat. Photonics* **2012**, *6*, 248–252. [CrossRef]
5. Gaafar, M.A.; Jalas, D.; Faolain, L.O.; Li, J.; Krauss, T.F.; Petrov, A.Y.; Eich, M. Reflection from a free carrier front via an intraband indirect photonic transition. *Nat. Commun.* **2018**, *9*, 1447. [CrossRef]
6. Li, X.; Liao, J.; Nie, Y.; Marko, M.; Jia, H.; Liu, J.; Wang, X.; Wong, C.W. Unambiguous demonstration of soliton evolution in slow-light silicon photonic crystal waveguides with SFG-XFROG. *Opt. Express* **2015**, *23*, 10282. [CrossRef] [PubMed]
7. Blanco-Redondo, A.; de Sterke, C.M.; Sipe, J.E.; Krauss, T.F.; Eggleton, B.J.; Husko, C. Pure-quartic solitons. *Nat. Commun.* **2016**, *7*, 10427. [CrossRef]
8. Colman, P.; Husko, C.; Combri, S.; Sagnes, I.; Wong, C.W.; Rossi, A.D. Temporal solitons and pulse compression in photonic crystal waveguides. *Nat. Photonics* **2010**, *4*, 862–868. [CrossRef]
9. Kondo, K.; Shinkawa, M.; Hamachi, Y.; Saito, Y.; Arita, Y.; Baba, T. Ultrafast slow-light tuning beyond the carrier lifetime using photonic crystal waveguides. *Phys. Rev. Lett.* **2013**, *110*, 53902. [CrossRef] [PubMed]
10. Kondo, K.; Baba, T. Slow-light-induced Doppler shift in photonic-crystal waveguides. *Phys. Rev. A* **2016**, *93*, 11802. [CrossRef]
11. Kondo, K.; Baba, T. On-chip autocorrelator using counter-propagating slow light in a photonic crystal with two-photon absorption photodiodes. *Optica* **2017**, *4*, 1109–1112. [CrossRef]
12. Konoike, R.; Nakagawa, H.; Nakadai, M.; Asano, T.; Tanaka, Y.; Noda, S. On-demand transfer of trapped photons on a chip. *Sci. Adv.* **2016**, *2*, 1109–1112. [CrossRef]
13. Colman, P.; Combrié, S.; Lehoucq, G.; De, R.A. Control of dispersion in photonic crystal waveguides using group symmetry theory. *Opt. Express* **2012**, *20*, 13108–13114. [CrossRef]
14. Notomi, M.; Yamada, K.; Shinya, A.; Takahashi, J.; Takahashi, C.; Yokohama, I. Extremely large group-velocity dispersion of line-defect waveguides in photonic crystal slabs. *Phys. Rev. Lett.* **2001**, *87*, 253902. [CrossRef]
15. Frandsen, L.H.; Lavrinenko, A.V.; Jacob, F.P.; Borel, P.I. Photonic crystal waveguides with semi-slow light and tailored dispersion properties. *Opt. Express* **2006**, *14*, 9444–9450. [CrossRef]
16. Kubo, S.; Mori, D.; Baba, T. Low-group-velocity and low-dispersion slow light in photonic crystal waveguides. *Opt. Lett.* **2007**, *32*, 2981–2983. [CrossRef] [PubMed]

17. Mori, D.; Baba, T. Wideband and low dispersion slow light by chirped photonic crystal coupled waveguide. *Opt. Express* **2005**, *13*, 9398–9408. [CrossRef]
18. Han, X.; Wang, T.; Tang, J.; Liu, B.; Wang, B.; He, Y.; Zhu, Y. Slow light with large group index bandwidth product in ellipse-hole photonic crystal waveguides. *Appl. Opt.* **2015**, *54*, 1543–1547. [CrossRef] [PubMed]
19. Vercruysse, D.; Sapra, N.V.; Su, L.; Jelena, V. Dispersion Engineering With Photonic Inverse Design. *IEEE J. Sel. Top. Quant.* **2020**, *26*, 1–6. [CrossRef]
20. Wu, H.; Han, S.; Li, F.; Yang, Z. Slow light with high normalized delay–bandwidth product in organic photonic crystal coupled-cavity waveguide. *Appl. Opt.* **2020**, *59*, 642–647. [CrossRef] [PubMed]
21. Mann, N.; Combrie, S.; Colman, P.; Patterson, M.; Rossi, A.D.; Hughes, S. Reducing disorder-induced losses for slow light photonic crystal waveguides through Bloch mode engineering. *Opt. Lett.* **2013**, *38*, 4244–4247. [CrossRef]
22. Zhou, H.; Huang, S.; Li, X.; McMillan, J.F.; Zhang, C.; Wong, K.K.; Yu, M.; Lo, G.; Kwong, D.; Qiu, K.; et al. Real-time dynamics and cross-correlation gating spectroscopy of free-carrier Drude slow-light solitons. *Light. Sci. Appl.* **2017**, *6*, e17008. [CrossRef] [PubMed]
23. Agrawal, G.P. *Nonlinear Fiber Optics*, 6th ed.; Academic Press: Cambridge, MA, USA, 2019.
24. Hu, S.; Khater, M.; Salas-Montiel, R.; Kratschmer, E.; Engelmann, S.; Green, W.M.J.; Weiss, S.M. Experimental realization of deep-subwavelength confinement in dielectric optical resonators. *Sci. Adv.* **2018**, *4*, t2355. [CrossRef] [PubMed]
25. Johnson, S.G.; Joannopoulos, J.D. Block-iterative frequency-domain methods for Maxwell's equations in a planewave basis. *Opt. Express* **2001**, *8*, 173–190. [CrossRef]
26. Manual-MPB Documentation. Available online: https://mpb.readthedocs.io/en/latest/ (accessed on 31 March 2021).
27. Yohei, H.; Shousaku, K.; Toshihiko, B. Slow light with low dispersion and nonlinear enhancement in a lattice-shifted photonic crystal waveguide. *Opt. Lett.* 2009, *34*, 1072–1074.
28. Joannopoulos, J.D.; Johnson, S.G.; Winn, J.N.; Meade, R.D. *Photonic Crystals: Molding the Flow of Light*, 2nd ed.; Princeton University Press: Princeton, NJ, USA, 2008.
29. Serna, S.; Colman, P.; Zhang, W.; Roux, X.L.; Caer, C.; Vivien, L.; Cassan, E. Experimental GVD engineering in slow light slot photonic crystal waveguides. *Sci. Rep.* **2016**, *6*, 26956. [CrossRef] [PubMed]
30. Fu, M.; Liao, J.; Shao, Z.; Marko, M.; Zhang, Y.; Wang, X.; Li, X. Finely engineered slow light photonic crystal waveguides for efficient wideband wavelength-independent higher-order temporal solitons. *Appl. Opt.* **2016**, *55*, 3740–3745. [CrossRef]
31. Hao, R.; Cassan, E.; Kurt, H.; Roux, X.L.; Marris-Morini, D.; Vivien, L.; Wu, H.; Zhou, Z.; Zhang, X. Novel slow light waveguide with controllable delay-bandwidth product and utra-low dispersion. *Opt. Express* **2010**, *18*, 5942–5950. [CrossRef] [PubMed]